LETTER

Random anti–lasing through coherent perfect absorption in a disordered medium

Kevin Pichler[1], Matthias Kühmayer[1], Julian Böhm[2], Andre Brandstötter[1], Philipp Ambichl[1], Ulrich Kuhl[2,3]* & Stefan Rotter[1,3]*

Non-Hermitian wave engineering is a recent and fast-moving field that examines both fundamental and application-oriented phenomena[1–7]. One such phenomenon is coherent perfect absorption[8–11]—an effect commonly referred to as 'anti-lasing' because it corresponds to the time-reversed process of coherent emission of radiation at the lasing threshold (where all radiation losses are exactly balanced by the optical gain). Coherent perfect absorbers (CPAs) have been experimentally realized in several setups[10–18], with the notable exception of a CPA in a disordered medium (a medium without engineered structure). Such a 'random CPA' would be the time-reverse of a 'random laser'[19,20], in which light is resonantly enhanced by multiple scattering inside a disorder. Because of the complexity of this scattering process, the light field emitted by a random laser is also spatially complex and not focused like a regular laser beam. Realizing a random CPA (or 'random anti-laser') is therefore challenging because it requires the equivalent of time-reversing such a light field in all its degrees of freedom to create coherent radiation that is perfectly absorbed when impinging on a disordered medium. Here we use microwave technology to build a random anti-laser and demonstrate its ability to absorb suitably engineered incoming radiation fields with near-perfect efficiency. Because our approach to determining these field patterns is based solely on far-field measurements of the scattering properties of a disordered medium, it could be suitable for other applications in which waves need to be perfectly focused, routed or absorbed.

The absorption of radiation is a goal with many applications, from the spectral filtering of electromagnetic signals to the conversion of sunlight into heat. It has recently been discovered that in principle any object can be turned into a CPA at well-defined frequencies, provided that its absorption strength and the wavefront of the incoming radiation are suitably adjusted[8,11]—an effect of both fundamental and technological relevance. Easily controllable systems with a simple geometrical structure, such as a slab of silicon irradiated by two suitably adjusted laser beams on either side, have already provided experimental proof of principle for this intriguing effect[10]. Theory predicts[8,11], however, that coherent perfect absorption is a general phenomenon that can also be realized in media without any predesigned geometrical form or arrangement and with waves for which not only one or two, but many degrees of freedom need to be adjusted. The ultimate example of such a medium is a disordered structure with a small absorbing element embedded in its middle[21] (see Fig. 1). Although in this case the radiation impinging from outside first has to penetrate a scattering layer to reach the absorber, surprisingly the absorption can still be perfect, such that the incident wave is fully dissipated by the absorber and no part of it gets back-reflected to the exterior. The unique radiation state realized in this way is the exact time-reverse of a random laser mode brought to its specific lasing threshold by replacing the small absorber by a gain element of equal size, but with an amplification rate that is exactly opposite to the dissipation rate of the absorber.

A straightforward way to realize such a random anti-laser would be to use wavefront-shaping techniques, in which enormous progress has been made recently[22,23]. The challenge and the reason why the implementation of random anti-lasing has remained out of reach so far is that it requires a very challenging level of control. First, one has to identify discrete pairs of values for the absorption strength and for the radiation frequency at which a CPA can be realized. Then, at each of these isolated CPA points, both the amplitudes and the phases of all relevant pixels that determine the complex speckle pattern of a random anti-laser mode in its far field need to be adjusted to reach perfect absorption. Away from these CPA points, reaching perfect absorption is impossible in principle. This full level of control also sets our work apart from previous implementations in which the wave field alone was optimized in several of its asymptotic components to increase the absorption at a specific target, such as a receiving antenna in a complex environment[21,24–26]. Instead of providing a quantitative improvement with respect to earlier studies, here we demonstrate how to reach the optimum degree of absorption with an approach that is both scalable in terms of the number of pixels and readily transferrable to other experimental platforms.

Our starting point is to place a disordered medium inside a waveguide that supports a finite number of transverse modes, which in turn
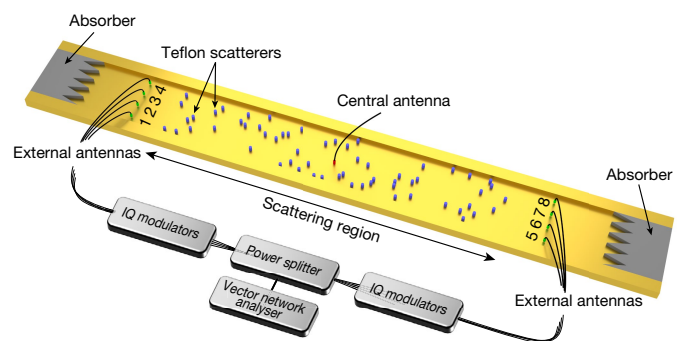

Fig. 1 | Experimental setup of the random anti-laser. Microwaves of a well-defined frequency are generated by a vector network analyser and equally distributed by a power splitter to eight in-phase/quadrature (IQ) modulators, where the amplitudes and relative phases of the signals are independently tuned. These signals are injected into an aluminium waveguide via eight external antennas (four on each side, numbered as indicated). Absorbers are placed at the waveguide ends to avoid back-reflection of the injected and transmitted signals. The central scattering region of the waveguide contains a disordered medium consisting of a set of randomly placed Teflon scatterers. Localized absorption is introduced to the system by placing a monopole antenna with a 50-Ω resistance in the middle of the disordered region (central antenna). The scattering matrix of the system is determined by measuring the field in the space between the scattering region and the external antennas using a movable antenna that can dip into the waveguide through a grid of holes in the top plate (not shown). The distances from the external antennas to the absorbers and to the scattering region are not to scale.

[1]Institute for Theoretical Physics, Vienna University of Technology (TU Wien), Vienna, Austria. [2]Institut de Physique de Nice, Université Côte d'Azur, CNRS, Nice, France. [3]These authors jointly supervised this work: Ulrich Kuhl, Stefan Rotter. *e-mail: ulrich.kuhl@unice.fr; stefan.rotter@tuwien.ac.at
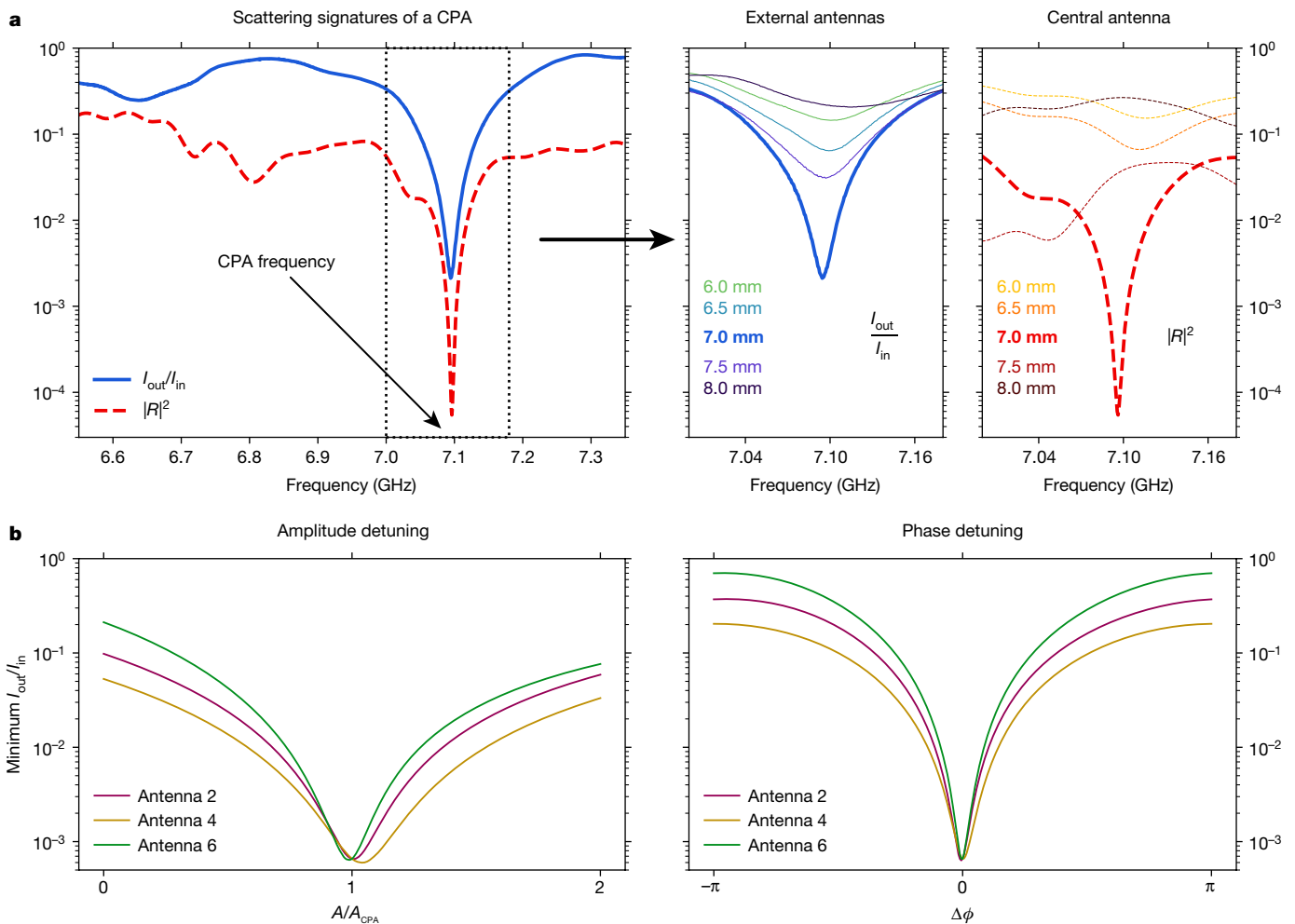
Fig. 2 | Analysis of a CPA state. a, Scattering signatures of a CPA state for a waveguide configuration with 60 scatterers; see Fig. 1. The quantities I_{in} and I_{out} denote the incoming and outgoing intensity of the injected CPA state, measured outside the disordered region, and R is the reflection signal, measured at the central antenna when microwaves are injected there (see also Extended Data Fig. 1). Close to the CPA frequency of around 7.1 GHz, both the ratio I_{out}/I_{in} and the reflection coefficient $|R|^2$ show a pronounced minimum that depends very sensitively on the length of the central absorbing antenna. As shown in the two panels on the right, increasing the antenna length first increases the CPA absorption dip in both I_{out}/I_{in} and $|R|^2$ until a minimum is reached for an antenna length of

7 mm. For further extension of the length of the central antenna, both the reflection signal increases again and the absorption efficiency is decreased. **b**, Sensitivity of the CPA minimum to detunings in individual IQ modulators. We change the amplitude A (left) and phase ϕ (right) of exemplary input antennas while the signals at all other antennas remain as required for the CPA state (amplitude A_{CPA} and phase ϕ_{CPA}). Any of these detunings leads to a substantial deterioration of the efficient absorption at the CPA configuration. Results in **b** were generated by linear superposition of S-matrix data, whereas the blue curve in **a** is a direct measurement of the injected CPA state.

determines the required number of controllable degrees of freedom in the radiation field. Moreover, we present an innovative microwave measurement setup that enables us both to measure the entire scattering matrix of the disordered medium in a large frequency range and to inject the desired field pattern with near-perfect absorption in situ. Our setup, schematically depicted in Fig. 1, consists of a waveguide containing a disordered medium built of 60 randomly placed cylindrical Teflon scatterers with radius $r = 2.55$ mm. At an operation frequency between 6 GHz and 7.5 GHz, the waveguide supports four transverse modes, requiring four antennas on each side (left and right) to fully control the injected microwave field in both phase and amplitude. In the middle of the scattering region we insert a monopole antenna with a 50-Ω resistance attached, which provides a localized and very strong loss channel. In addition, the microwave field is subject to weak global absorption caused by the skin effect in the metallic waveguide and by escape through the small holes in the top plate (details about the experimental setup are provided in Methods and Supplementary Information). To control the degree of loss in situ—as is necessary for the realization of a CPA—we vary the length of the central absorbing antenna inside the waveguide, thus changing its coupling strength to

the system[27,28] (measurements of the length and frequency dependence of the antenna's coupling and absorption strength are presented in Supplementary Information section 3).

The crucial quantity to characterize the above system—both theoretically and in our experiment—is the scattering matrix (or S-matrix) S that relates the injected fields, ψ_{in}, to the outgoing ones, ψ_{out}, as $\psi_{out} = S\psi_{in}$ in all of the eight asymptotic waveguide channels. The unitary scattering matrix of a Hermitian system (without gain or loss) generally has zeroes in the upper half ($\mathrm{Im}(\nu) > 0$) and poles in the lower half ($\mathrm{Im}(\nu) < 0$) of the complex plane of frequency ν, symmetrically distributed around the real axis. The addition of gain or loss makes the system non-Hermitian and moves these zeroes and poles around in the complex frequency plane (including effects of frequency pulling due to dispersion in the gain or loss). Adding gain turns a disordered medium into a random laser as soon as the first S-matrix pole hits the real ν axis (which defines the lasing threshold). When loss is added, the medium turns into a random anti-laser (disordered CPA) at exactly those frequencies and loss values at which any of the S-matrix zeroes crosses the real ν axis[27,28]. Because above the lasing threshold nonlinear saturation effects stabilize the S-matrix poles on the real axis, but no
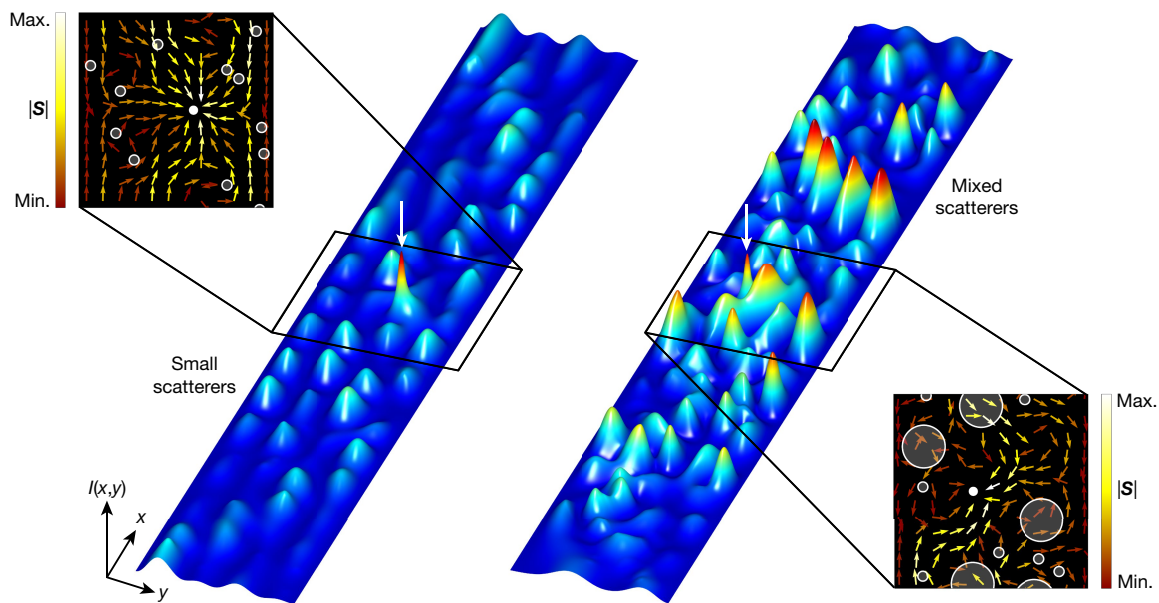
Fig. 3 | Field and flux patterns of CPA states. Microwave intensity of CPA states injected through the external antennas into a weakly disordered waveguide with 60 small scatterers (left) and a strongly disordered waveguide with 60 mixed-size scatterers (right). Shown are results of numerical simulations without global loss, where the colour scale ranges from low (blue) to high (red) intensity. The white arrow marks the position of the central absorbing antenna implemented as an absorbing scatterer in the simulations (see Methods). In the vicinity of the antenna the Poynting vector S has only inward-pointing components (see insets, in which white semi-transparent circles mark the scatterers and the filled white circle represents the absorbing antenna). We find quantitative agreement of these simulations with the experimental data (see Supplementary Information section 4). Flux patterns for the entire scattering region are provided in Extended Data Fig. 2 and an analysis of the microwave field in the absence of the central absorbing antenna is given in Extended Data Fig. 3.

equivalent effects are at work for the S-matrix zeroes of the anti-laser, the analogy between lasing and anti-lasing holds only on the linear level at the mode-specific lasing thresholds. At these discrete CPA points a random anti-laser mode ψ_{CPA} is an eigenstate of the scattering matrix S with eigenvalue $\lambda_{CPA} = 0$ such that $S\psi_{CPA} = 0$, where ψ_{CPA} is the incoming radiation field and the empty 0 field is the outgoing one. The expedient and robust approach that we deduce from this analysis is the following: we measure the S-matrix of the system in a frequency interval broad enough to contain many S-matrix zeroes and for a number of loss values of the central absorbing antenna that are strong enough to drag the zeroes with the smallest imaginary parts down to the real ν axis. After evaluating the eigenvalues of these different S-matrices, we identify those parameter configurations for which the absolute value of the smallest S-matrix eigenvalue dips almost to zero. We then inject the CPA eigenstate corresponding to this minimal eigenvalue into the system and evaluate its properties, in particular the degree of absorption associated with it.

Following this approach, we achieve more than 99.78% absorption of the injected intensity, as illustrated by the blue curve in Fig. 2a, in which we show the ratio between the outgoing and the incoming microwave intensity (I_{out}/I_{in}) of one specific CPA state, as measured in front of the eight external antennas. We emphasize the very pronounced minimum at the CPA frequency (where the CPA state was evaluated), which is a first and revealing hallmark of the effect that we are aiming for.

To check whether we have indeed realized a disordered CPA, rather than a coherent enhancement of absorption[29] or one of the previously implemented focusing schemes[21,24–26], we devised a number of independent tests. First, because we expect a CPA state to be primarily absorbed by the central absorbing antenna (and less by the metallic top and bottom plates in the waveguide)[30], the time-reverse of this state should be a harmonic microwave signal that enters through the central absorbing antenna without any back-reflection. In other words, we should find that the central antenna is critically coupled[31,32] to the disordered waveguide system at a frequency and antenna coupling strength that are very close to where we found the CPA independently. In our experiment such a time reversal (or phase-conjugation) is easy to implement, and we find that indeed microwave signals injected

through the central absorbing antenna show a pronounced dip in the frequency-dependent back-reflection coefficient $|R|^2$; see red dashed curve in Fig. 2a. The observed dip is only slightly shifted in frequency (by 0.025%) with respect to the dip of the CPA state found before. This shift is caused by experimental imperfections and by the weak global absorption in the system, because of which the two states discussed above are not exactly the time-reverse of each other (see also Supplementary Information section 7, in which we directly compare the CPA state with the time-reverse of a state injected through the central antenna).

We now investigate how these CPA minima change with respect to the coupling strength of the central antenna and to the phase and amplitude configuration of the injected CPA state. Because theory predicts that a CPA requires a zero of the S-matrix to be located on the real frequency axis, we should find a reduced amount of absorption not only for smaller, but also for larger antenna coupling; that is, when the S-matrix zero lies above or below the real axis, respectively. In our setup the change of antenna coupling is realized by varying the length of the central antenna inside the waveguide (see Supplementary Information section 3 for details) and we find that indeed not only a smaller, but also a larger coupling strength (corresponding to more loss) diminishes the resonant CPA minimum substantially; see right panels in Fig. 2a. Specifically, we find that an antenna extending 7 mm into the waveguide is optimal for the observed CPA state (the waveguide has an overall thickness of 8 mm between top and bottom plates). As shown in Supplementary Information section 6, this absorbing antenna length is also ideal for reaching a minimum in the S-matrix eigenvalue. To illustrate how accurately the CPA state must be adjusted in all eight external antennas, we check what happens when either the amplitude or the phase of just one of the eight antennas is detuned away from the configuration of the CPA state. As shown in Fig. 2b for antennas 2, 4, and 6, the CPA dip (that is, the minimum of the ratio I_{out}/I_{in} in the frequencies around 7.1 GHz) gets considerably shifted upwards by factors of up to approximately 10^3—a feature that illustrates how strongly the absorption in the system is controlled interferometrically, rather than by the mere presence of the absorbing antenna alone.
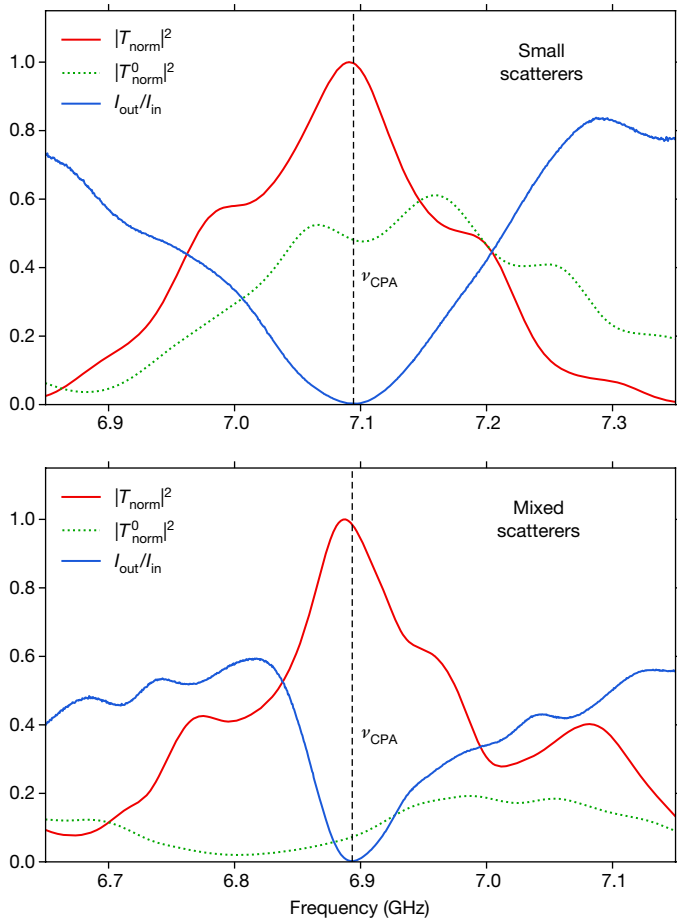
Fig. 4 | Transmission of CPA states into the central antenna. As an experimental signature of the simulated results presented in Fig. 3, we measure the transmission of the investigated CPA states into the absorbing antenna for configurations with 60 small (top) and 60 mixed-size (bottom) scatterers. Our data confirm that close to the CPA frequency ν_{CPA}, where the absorption of the CPA state is most efficient, the transmission to the absorbing antenna has its maximum. The plots compare the squared absolute value of the normalized transmission T_{norm} into the absorbing antenna with the ratio between the outgoing (I_{out}) and incoming (I_{in}) intensity of the CPA states. The transmission is normalized with respect to its maximum within the measured interval: $|T_{max}| = 0.017$ for the small scatterers and $|T_{max}| = 0.013$ for the mixed-size scatterers. These values are calibrated with respect to the flux injected into the power splitter, which is strongly attenuated before reaching the interior of the waveguide; see Methods for more details. As a reference measurement we also show the transmission T_{norm}^0 of these two CPA states into the absorbing antenna when all scatterers are removed from the waveguide (the same normalization $|T_{max}|$ is used here as for T_{norm}). Because the CPA states are customized for each specific scatterer configuration, the removal of the scatterers leads to a strong reduction of the transmission into the absorbing antenna.

Another distinguishing feature of the CPA states that we generate is contained in the microwave field pattern around the central antenna; see Fig. 3 (left). Owing to the near-perfect absorption, we expect that the flux associated with the CPA state (as given by the Poynting vector) has a predominantly inward-flowing component close to the central antenna. However, because the field is inaccessible experimentally in the direct vicinity of the central antenna, we reconstruct the entire scattering system numerically. Using a finite-element discretization on a two-dimensional mesh that maps the experimental system geometry—including all scatterer and antenna positions—without any fit parameters, we find the numerically evaluated CPA state to have 95.6% correlation with the experimentally realized one (see Supplementary Information section 4). This remarkable degree of agreement enables us to check the flux pattern associated with the CPA state in the numerical

results, which we find to be directed solely towards the absorbing antenna; see insets in Fig. 3.

Finally, we demonstrate that our approach is generally applicable also to disordered configurations with different scattering strengths. With both the scattering (l_s) and the transport (l_t) mean free paths for the disorder considered in Figs. 1, 2 being about twice as large ($l_s \approx l_t \approx 1.3$ m) as the length of the scattering region ($L = 0.6$ m), we are in the regime of weak scattering, where the disorder causes substantial aberrations but does not trap waves for very long times (see Supplementary Information section 8). To increase the scattering strength, we work with a mixture of 28 small and 32 large dielectric disks with radii of $r = 2.55$ mm and $r = 11$ mm, respectively, randomly placed in the central scattering region. With the larger disks being much closer in size to the operating wavelength of $\lambda \approx 43$ mm, both the scattering and the transport mean free paths are now strongly reduced below the length of the scattering region ($l_s \approx 0.08$ m $< l_t \approx 0.2$ m $< L = 0.6$ m). Also for this strongly scattering system we immediately find a pronounced CPA state with a ratio of $I_{out}/I_{in} = 2.1 \times 10^{-3}$ at the CPA frequency of 6.9 GHz; see Fig. 4 (bottom). Its numerically evaluated flux pattern is again fully directed towards the central antenna; see Fig. 3 (right). As an experimental signature of this behaviour, we also verify—both for the weak and for the strong scattering configuration—that the transmission into the central absorbing antenna has a maximum at the CPA frequency; see Fig. 4. These states are thus mostly absorbed by the central antenna and only weakly affected by the global loss in the waveguide. In Supplementary Information section 5 we also discuss CPA states in a strongly scattering system for which the absorption from the waveguide dominates over the absorption by the central antenna. The fact that we can detect and inject such unconventional CPA states demonstrates the versatility of our approach and that it in no way relies on a time-reversal operation using the central antenna as a source.

In summary we present the first experimental realization, to our knowledge, of a random anti-laser, which provides proof of principle that coherent perfect absorption can also be realized in arbitrarily composed systems such as disordered media. We emphasize that our approach requires only the multi-modal scattering matrix—neither any information on the inner structure of the medium nor a source placed inside of it is necessary. Our work is thus also relevant for practical applications, including perfect focusing of electromagnetic signals[24] and sound fields[25] in complex environments, such as in an office space or in biological tissue. On the conceptual level, we expect our results to serve as a bridge between the fields of wavefront shaping and non-Hermitian physics.

Online content

Any methods, additional references, Nature Research reporting summaries, source data, statements of data availability and associated accession codes are available at https://doi.org/10.1038/s41586-019-0971-3.

1. Berry, M. V. Physics of nonhermitian degeneracies. *Czech. J. Phys.* **54**, 1039–1047 (2004).
2. Bender, C. M. Making sense of non-Hermitian Hamiltonians. *Rep. Prog. Phys.* **70**, 947–1018 (2007).
3. Moiseyev, N. *Non-Hermitian Quantum Mechanics* (Cambridge Univ. Press, Cambridge, 2011).
4. Heiss, W. D. The physics of exceptional points. *J. Phys. A* **45**, 444016 (2012).
5. Feng, L., El-Ganainy, R. & Ge, L. Non-Hermitian photonics based on parity–time symmetry. *Nat. Photon.* **11**, 752–762 (2017).
6. Longhi, S. Parity-time symmetry meets photonics: a new twist in non-Hermitian optics. *Europhys. Lett.* **120**, 64001 (2017).
7. El-Ganainy, R. et al. Non-Hermitian physics and PT symmetry. *Nat. Phys.* **14**, 11–19 (2018).
8. Chong, Y. D., Ge, L., Cao, H. & Stone, A. D. Coherent perfect absorbers: time-reversed lasers. *Phys. Rev. Lett.* **105**, 053901 (2010).
9. Longhi, S. PT-symmetric laser absorber. *Phys. Rev. A* **82**, 031801 (2010).
10. Wan, W. et al. Time-reversed lasing and interferometric control of absorption. *Science* **331**, 889–892 (2011).
11. Baranov, D. G., Krasnok, A., Shegai, T., Alù, A. & Chong, Y. Coherent perfect absorbers: linear control of light with light. *Nat. Rev. Mater.* **2**, 17064 (2017).

12. Pu, M. et al. Ultrathin broadband nearly perfect absorber with symmetrical coherent illumination. *Opt. Express* **20**, 2246–2254 (2012).
13. Bruck, R. & Muskens, O. L. Plasmonic nanoantennas as integrated coherent perfect absorbers on SOI waveguides for modulators and all-optical switches. *Opt. Express* **21**, 27652 (2013).
14. Sun, Y., Tan, W., Li, H., Li, J. & Chen, H. Experimental demonstration of a coherent perfect absorber with PT phase transition. *Phys. Rev. Lett.* **112**, 143903 (2014).
15. Roger, T. et al. Coherent perfect absorption in deeply subwavelength films in the single-photon regime. *Nat. Commun.* **6**, 7031 (2015).
16. Wong, Z. J. et al. Lasing and anti-lasing in a single cavity. *Nat. Photon.* **10**, 796–801 (2016).
17. Meng, C., Zhang, X., Tang, S. T., Yang, M. & Yang, Z. Acoustic coherent perfect absorbers as sensitive null detectors. *Sci. Rep.* **7**, 43574 (2017).
18. Richoux, O., Achilleos, V., Theocharis, G. & Brouzos, I. Subwavelength interferometric control of absorption in three-port acoustic network. *Sci. Rep.* **8**, 12328 (2018).
19. Cao, H. Lasing in random media. *Waves Random Media* **13**, R1–R39 (2003).
20. Wiersma, D. S. The physics and applications of random lasers. *Nat. Phys.* **4**, 359–367 (2008).
21. Lerosey, G., de Rosny, J., Tourin, A. & Fink, M. Focusing beyond the diffraction limit with far-field time reversal. *Science* **315**, 1120–1122 (2007).
22. Mosk, A. P., Lagendijk, A., Lerosey, G. & Fink, M. Controlling waves in space and time for imaging and focusing in complex media. *Nat. Photon.* **6**, 283–292 (2012).
23. Rotter, S. & Gigan, S. Light fields in complex media: mesoscopic scattering meets wave control. *Rev. Mod. Phys.* **89**, 015005 (2017).
24. Kaina, N., Dupré, M., Lerosey, G. & Fink, M. Shaping complex microwave fields in reverberating media with binary tunable metasurfaces. *Sci. Rep.* **4**, 6693 (2015); erratum **5**, 7966 (2015).
25. Ma, G., Fan, X., Sheng, P. & Fink, M. Shaping reverberating sound fields with an actively tunable metasurface. *Proc. Natl Acad. Sci. USA* **115**, 6638–6643 (2018).
26. Gerlach, D. & Paulraj, A. Base station transmitting antenna arrays for multipath environments. *Signal Process.* **54**, 59–73 (1996).
27. Li, H., Suwunnarat, S., Fleischmann, R., Schanz, H. & Kottos, T. Random matrix theory approach to chaotic coherent perfect absorbers. *Phys. Rev. Lett.* **118**, 044101 (2017).
28. Fyodorov, Y. V., Suwunnarat, S. & Kottos, T. Distribution of zeros of the S matrix of chaotic cavities with localized losses and coherent perfect absorption: non-perturbative results. *J. Phys. A* **50**, 30LT01 (2017).
29. Chong, Y. D. & Stone, A. D. Hidden black: coherent enhancement of absorption in strongly scattering media. *Phys. Rev. Lett.* **107**, 163901 (2011).
30. Jackson, J. D. *Classical electrodynamics* (John Wiley & Sons, New York, 2009).
31. Cai, M., Painter, O. & Vahala, K. J. Observation of critical coupling in a fiber taper to a silica-microsphere whispering-gallery mode system. *Phys. Rev. Lett.* **85**, 74–77 (2000).
32. Tischler, J. R., Bradley, M. S. & Bulović, V. Critically coupled resonators in vertical geometry using a planar mirror and a 5 nm thick absorbing film. *Opt. Lett.* **31**, 2045–2047 (2006).

Author contributions Measurements and data evaluation were carried out by K.P. under the supervision of U.K. J.B. and U.K. designed the experimental setup. S.R. proposed the project and supervised the theoretical and numerical tasks carried out by M.K., K.P., A.B. and P.A. K.P. and S.R. wrote the manuscript with input from all authors.

Competing interests The authors declare no competing interests.

Additional information
Extended data is available for this paper at https://doi.org/10.1038/s41586-019-0971-3.
Supplementary information is available for this paper at https://doi.org/10.1038/s41586-019-0971-3.
Reprints and permissions information is available at http://www.nature.com/reprints.
Correspondence and requests for materials should be addressed to U.K. or S.R.
Publisher's note: Springer Nature remains neutral with regard to jurisdictional claims in published maps and institutional affiliations.

METHODS

Experimental setup. Our experimental setup consists of a rectangular aluminium waveguide of 10 cm inner width (y direction), 8 mm inner height (z direction) and 238 cm total length (x direction). Microwaves can be injected into the system via eight antennas reaching about 3 mm into the waveguide (weak coupling), four on each side (see Fig. 1). The signal is generated by a vector network analyser (VNA) and equally distributed by a power splitter to eight IQ modulators, where the amplitudes and relative phases of the injected microwaves are controlled and then transferred to the eight antennas. Absorbers are placed at both ends of the waveguide to avoid back-reflection of the injected and transmitted signals. The central scattering region (length, 60 cm) of the waveguide contains the disordered medium, which is realized in our case by a set of randomly placed cylindrical Teflon scatterers (index of refraction, $n = 1.44$). Two different sizes of scatterers are used (radii, 2.55 mm and 11 mm; height, 8 mm). As a localized absorber we use a monopole antenna with a 50-Ω resistance attached. This absorbing antenna is placed at the centre of the system regarding its x position and slightly out of centre (± 9 mm) regarding its y position. The field inside the waveguide can be measured by a movable antenna, which can dip into the waveguide through a grid of holes (spacing of 5 mm from centre to centre) in the top plate of the waveguide. This probe antenna has only a small effect on the field that it measures because it reaches only 4 mm into the waveguide and its absorption is therefore around 1.5 orders of magnitude weaker than that of the central absorbing antenna. This estimate is based on a comparison of the transmission from the external antennas to the probe antenna placed in the vicinity of the absorbing antenna with the transmission to the absorbing antenna itself. Another indirect and independent confirmation of the negligible effect of the probe antenna on the field is the fact that the scattering matrix that we evaluate with it predicts the correct positions of the CPA points, as confirmed by the near-perfect absorption that we find when injecting the CPA states in situ.

Measurement settings. Our measurements were performed in the frequency range from 6 GHz to 7.5 GHz (at 2,501 equidistant frequency points) with the same VNA as that used to generate the signals. This frequency range coincides with the interval in which exactly four modes can propagate freely through the empty waveguide. Data close to the mode openings (at 6 GHz and 7.5 GHz) are, however, not taken into account to avoid the influence of evanescent waveguide modes (restricting us to the spectral interval between 6.55 GHz and 7.35 GHz). For the measurement of the reflection signal at the central antenna, one port of the VNA is connected to this antenna, where it injects a signal and simultaneously measures its back-reflection. Evaluating the scattering matrix requires a measurement of the stationary field at both ends of the scattering region in the waveguide (see details below). Thus, for such measurements, one port of the VNA is used as the signal source for the external input antennas and another port is connected to the movable antenna, which is used for the field measurement. The same VNA port configuration is used for the injection and verification of the CPA states afterwards and for the measurement of the field around the absorbing antenna (only the very close vicinity of the central antenna remained inaccessible). We can also measure the field of the scattering state created when injecting microwaves through the central antenna by connecting one port to this antenna and the other port to the movable antenna. The transmission of the incoming CPA states into the central antenna is measured with one port as the signal source for the external antennas and another port connected to the central antenna. For the interpretation of the measured transmission values (S_{12} measurements; see legend of Fig. 4) of a CPA state into the absorbing antenna the whole path between the points of calibration has to be taken into account. In our case, the calibration is performed at the ends of the analyser cables, one of which is attached to the power splitter and the other to the central antenna for the transmission measurements. The signal injected into the system is then attenuated owing to the insertion loss in the power splitter and in the IQ modulators and because of the loss in the semi-rigid cables connecting the power splitter to the IQ modulators and in the flexible cables connecting the IQ modulators to the external antennas. We measure the transmission through this path for one IQ modulator (using the 0-dB attenuation adjustment) and find that the transmission through the power splitter, the semi-rigid cable, the IQ modulator and the flexible cable leading to the corresponding external antenna is given by $|S_{12}| \equiv |T| = 0.096$. The total transmission when using all of the eight IQ modulators at 0-dB attenuation would then be eight times this value, that is, $|T| = 0.768$. In addition to this intrinsic loss, the signal is deliberately attenuated at each IQ modulator, as required to create a certain CPA state, which leads to an additional average amplitude attenuation of about 44% for the CPA state corresponding to the configuration with 60 small scatterers presented in the main text. Because the external antennas emit symmetrically to the left and right, only half of the emitted intensity is actually injected towards the centre of the waveguide. In contrast to the central antenna, which is perfectly coupled at the CPA frequency, the external antennas extend only about 3 mm into the waveguide and are therefore weakly coupled, which further decreases the injected power. All of these effects do not have any influence on the field or flux patterns inside the system, but only reduce the global intensity. Also,

in the S-matrix measurements these effects cancel out because both the incoming and the outgoing fields are measured with the same antenna. Only in the case of transmission from the external region into the central absorbing antenna, where different antennas are used on either side, is the overall calibration more involved, and we use the flux injected into the power splitter as a reference (see legend of Fig. 4).

Control of the input state. One of the most important prerequisites to realize a CPA is to be in full control of the corresponding input state. Because we use four input antennas on each side of the waveguide, we are in the position to control all of the four available incoming modes from left and right. To inject a specific state into the system, the amplitudes and relative phases of the signals at each input antenna have to be adjusted properly by the IQ modulators. For this purpose, the relation between the IQ modulator settings and the resulting incoming waves needs to be identified. We do this by assigning to each IQ modulator a basis vector in the 'IQ modulator basis', which means that the respective IQ modulator is set to full transmission and relative phase zero while all other IQ modulators are set to maximum attenuation. For each of these basis vectors one has to determine the resulting composition of the incoming modes, which is done by measuring the field along the y direction for two different positions in the x direction, on each side of the scattering region. Along the y direction the field has to be measured at least at as many different positions as there are modes that need to be controlled (in our case, four on each side). To reduce noise effects, the field is measured at nine positions (our setup allows up to 19 different positions in the y direction). Because the field is a linear superposition of the incoming and outgoing modes, the measured mode coefficients $a_{\mathrm{meas},j}$, which are determined by means of a sine transformation of the complex measured field, satisfy the following relations with the coefficients for the incoming and outgoing modes ($a_{\mathrm{in},j}$ and $a_{\mathrm{out},j}$)

$$a_{\mathrm{meas},j}(x) = a_{\mathrm{in},j}e^{-ik_{\mathrm{x},j}x} + a_{\mathrm{out},j}e^{ik_{\mathrm{x},j}x}$$

$$a_{\mathrm{meas},j}(x + \mathrm{d}x) = a_{\mathrm{in},j}e^{-ik_{\mathrm{x},j}(x+\mathrm{d}x)} + a_{\mathrm{out},j}e^{ik_{\mathrm{x},j}(x+\mathrm{d}x)}$$

where j is the number of the respective mode and $k_{\mathrm{x},j} = \sqrt{k^2 - k_{\mathrm{y},j}^2}$, where $k = 2\pi\nu/c$, $k_{\mathrm{y},j} = j\pi/d$, ν is the frequency of the incoming waves, c is the speed of light, and d is the width of the waveguide in the y direction. If the coefficients of the incoming modes for each IQ modulator basis vector are written as columns in a matrix, the columns of the inverse of this matrix contain the coefficients $c_{m,j}$, by which the signals at the IQ modulators (numbered by m) have to be multiplied to get the desired mode j. A test of this procedure can be found in Supplementary Information section 1.

Evaluation of the scattering matrix. Because our approach to finding a potential CPA state requires an evaluation of an S-matrix eigenstate with vanishing eigenvalue, we first need to get access to the S-matrix of the system itself. The S-matrix represents a linear map of the incoming to the outgoing (flux-normalized) modes of the system

$$\boldsymbol{a}_{\mathrm{out}} = S \; \boldsymbol{a}_{\mathrm{in}}$$

which comprises N linearly independent equations for the N^2 elements of the S-matrix, where N is the total number of modes considered (eight in the experiment). One therefore needs to have at least N linearly independent sets of the coefficients $\boldsymbol{a}_{\mathrm{in}}$ and $\boldsymbol{a}_{\mathrm{out}}$ for all modes to get N^2 coupled equations for the S-matrix elements. Similarly to what is described in the section 'Control of the input state', this is most easily achieved by measuring the field at both ends of the scattering region on a grid of at least two different positions in the x direction and at least $N/2$ positions in the y direction, with one IQ modulator set to full transmission and all the others set to maximum attenuation, and repeating the measurement for each IQ modulator. Consequently, the same measurement data can be used to calculate both the IQ modulator settings and the scattering matrix of the system. In Supplementary Information section 2, we present typical examples of S-matrices for different system configurations.

Numerical simulations. In the experiment, the waveguide is enclosed between two plates at the bottom and the top (the latter is not shown in Fig. 1). In the considered frequency range only the lowest transverse mode is open in the 8 mm gap between these two plates (in the z direction). Owing to this strong mode confinement, our numerical simulations can be carried out in just two dimensions. We thus solve a two-dimensional scalar Helmholtz equation $[\Delta + n^2(\mathbf{r})k_0^2]\psi(\mathbf{r}) = 0$ for the transverse electric polarization using a finite-element method (NGSolve Finite Element Library, https://ngsolve.org/), where Δ is the Laplacian in two dimensions, $n(\mathbf{r})$ is the refractive index distribution dependent on the position $\mathbf{r} = (x, y)$, $k_0 = 2\pi/\lambda$ is the vacuum wavenumber and $\psi(\mathbf{r})$ is the z component of the electric field. We apply hard wall boundary conditions at the perimeter of the waveguide. In the asymptotic regions, where the external antennas are placed, we assume infinitely extended leads (implemented through 'perfectly matched layers'

placed at both ends of the waveguide). The central antenna in the middle of the waveguide is modelled by an absorbing scatterer of the same diameter as the antenna ($d = 4$ mm). The antenna coupling strength, which is experimentally controlled by the penetration depth into the waveguide, can be adjusted by the real and imaginary parts of the scatterer's refractive index. To find the point of coherent perfect absorption numerically, we perform a parameter scan over the real and imaginary parts of the absorbing scatterer's refractive index for both configurations considered in the main text, where we use the frequency of the experimental CPA state as a given parameter. Figure 3 shows the resulting numerical CPA states for the two different scattering configurations, where in both cases the absolute values of the corresponding eigenvalues of the scattering matrix are smaller than 10^{-10}. Our numerical results also show that for the CPA states that mostly couple out by the central antenna, the influence of global absorption in the weakly dissipative

waveguide plates and of the flux escaping through the holes in the top plate are barely noticeable. In Supplementary Information section 4 we provide more details on these aspects and a direct comparison between the numerical and experimental intensity distributions. In Supplementary Information section 5 we also discuss another set of CPA states in a strongly scattering system that are mostly absorbed by the global loss in the waveguide and only weakly affected by the central antenna. **Code availability.** For all our numerical simulations we used the NGSolve Finite Element Library (https://ngsolve.org/), a publicly available open-source software package.

Data availability
The data that support the findings of this study are available from the corresponding authors upon reasonable request.

Central antenna coupling
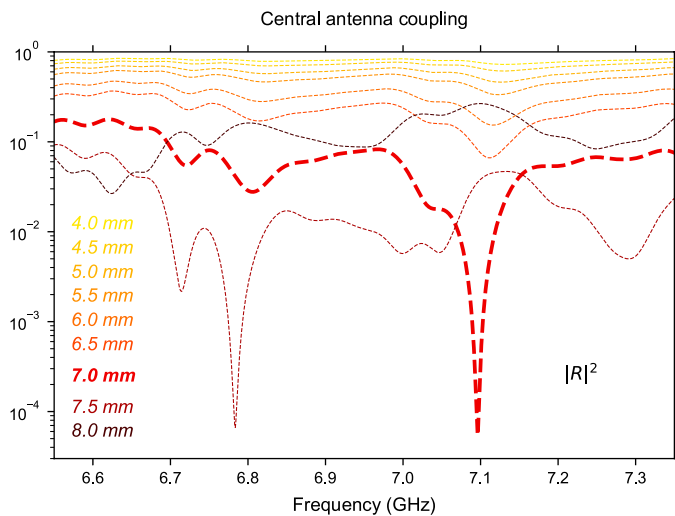
Extended Data Fig. 1 | Central antenna coupling. The plot shows the reflection signal $|R|^2$ measured for injection at the central antenna as a function of the signal frequency for different antenna lengths in the disordered configuration with 60 small scatterers shown in Fig. 1. One observes very clearly that at certain frequencies, pronounced minima of the reflection signal, and therefore maxima in the coupling efficiency of the antenna occur. For increasing antenna length these minima become lower until an optimal length is reached that is specific to each minimum (corresponding to 'critical coupling'). By further increasing the antenna length, the coupling efficiency decreases again. For the minimum in the frequency range around 7.1 GHz (see also main text) the optimal antenna length is 7 mm, whereas in the range around 6.8 GHz a length of 7.5 mm provides the highest coupling efficiency.
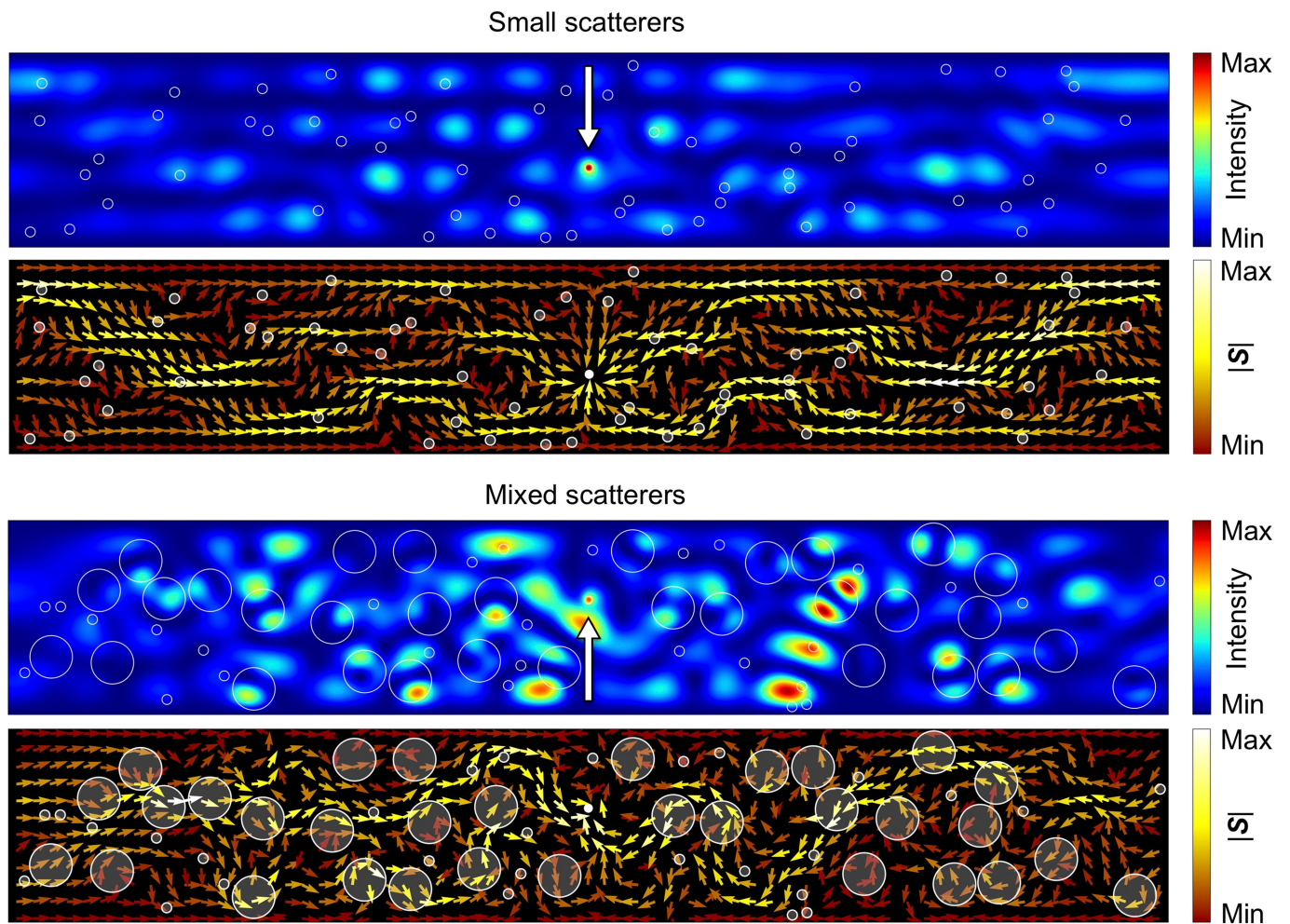
Extended Data Fig. 2 | Simulated energy-flux distribution in the entire scattering region. As a complement to Fig. 3, we provide here not only the simulated intensity (top panels) but also the Poynting vector (bottom panels) of the CPA states in the entire scattering region. In the top panels scatterers are displayed as white circles, with the white arrow indicating the position of the absorbing scatterer (that is, the central antenna), whereas in the bottom panels semi-transparent circles mark the scatterers and the filled circle represents the central antenna. For clarity, we plot the Poynting vectors on a different grid of points from that used in the insets in Fig. 3.
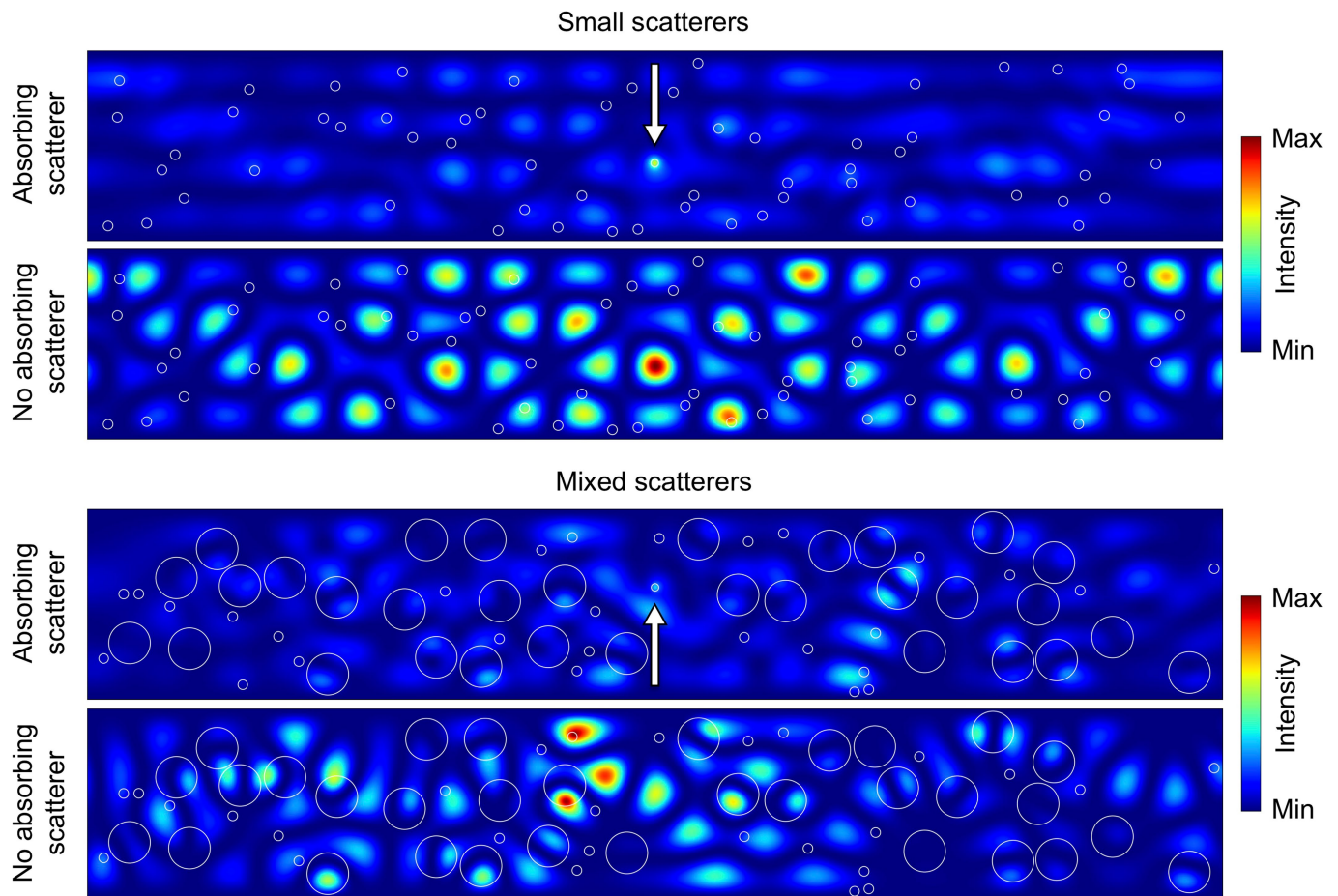
Extended Data Fig. 3 | Simulated intensity distribution in the presence and absence of the absorbing antenna. To illustrate the effect of the absorbing scatterer (that is, the central antenna) on the microwave field, we compare the simulated intensity distributions of the CPA states discussed in the main text, injected here in the presence (top panels) and absence (bottom panels) of this absorber (all other parameters and the colour scale stay unchanged). The white arrow indicates the antenna position and white circles represent the scatterers. One can clearly observe that removing the absorbing scatterer causes considerably higher and differently distributed intensity maxima in the waveguide, stemming from additional interference contributions of the waves that are no longer absorbed by the antenna.